Inorganic Chemistry

Article

pubs.acs.org/IC

Stabilizing Divalent Europium in Aqueous Solution Using Size-Discrimination and Electrostatic Effects

Martín Regueiro-Figueroa,[†] José Luis Barriada,[‡] Agnès Pallier,[§] David Esteban-Gómez,[†] Andrés de Blas,[†] Teresa Rodríguez-Blas,[†] Éva Tóth,[§] and Carlos Platas-Iglesias*[,†]

[†]Departamento de Química Fundamental, Universidade da Coruña, Campus da Zapateira, Rúa da Fraga 10, 15008 A Coruña, Spain

[‡]Departamento de Química Física e Enxeñaría Química I, Universidade da Coruña, Campus da Zapateira, Rúa da Fraga 10, 15008 A Coruña, Spain

[§]Centre de Biophysique Moléculaire, CNRS, Rue Charles Sadron, 45071 Orléans, Cedex 2, France

Supporting Information

ABSTRACT: We report two macrocyclic ligands containing a 1,10-diaza-18-crown-6 fragment functionalized with either two picolinamide pendant arms (bpa18c6) or one picolinamide and one picolinate arm (ppa18c6$^-$). The X-ray structure of $[La(ppa18c6)(H_2O)]^{2+}$ shows that the ligand binds to the metal ion using the six donor atoms of the crown moiety and the four donor atoms of the pendant arms, 11-coordination being completed by the presence of a coordinated water molecule. The X-ray structure of the $[Sr(bpa18c6)(H_2O)]^{2+}$ was also investigated due to the very similar ionic radii of Sr^{2+} and Eu^{2+}. The structure of this complex is very similar to that of $[La(ppa18c6)(H_2O)]^{2+}$, with the metal ion being 11-coordinated. Potentiometric measurements were used to determine the stability constants of the complexes formed with La^{3+} and Eu^{3+}. Both ligands present a very high selectivity for the large La^{3+} ion over the smaller Eu^{3+}, with a size-discrimination ability that exceeds that of the analogous ligand containing two picolinate pendant arms reported previously (bp18c6^{2-}). DFT calculations using the TPSSh functional and the large-core pseudopotential approximation provided stability trends in good agreement with the experimental values, indicating that charge neutral ligands derived from 1,10-diaza-18-crown-6 enhance the selectivity of the ligand for the large Ln^{3+} ions. Cyclic voltammetry measurements show that the stabilization of Eu^{2+} by these ligands follows the sequence bp18c6^{2-} < ppa18c6$^-$ < bpa18c6 with half-wave potentials of −753 mV (bp18c6^{2-}), −610 mV (ppa18c6$^-$), and −453 mV (bpa18c6) versus Ag/AgCl. These values reveal that the complex of bpa18c6 possesses higher stability against oxidation than the aquated ion, for which an $E_{1/2}$ value of −585 mV has been measured.

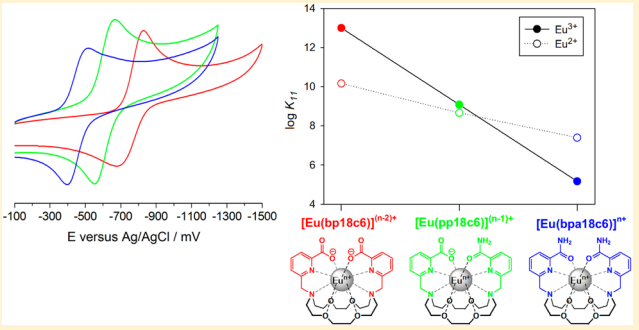

INTRODUCTION

The trivalent state is the most stable oxidation state of the lanthanides in aqueous solution, with the different Ln^{3+} ions having very similar coordination chemistry. From this perspective, the main difference between the Ln^{3+} ions is the monotonous contraction of the ionic radius on proceeding to the right across the 4f period (lanthanide contraction).[1] Among the different lanthanides, only Eu^{2+}, Yb^{2+}, and Sm^{2+} can be produced in aqueous media by reduction of the trivalent ions, but the latter two are oxidized very rapidly.[2] However, Eu^{2+} can persist in solution for some time, as its oxidation is relatively slow, and can be further stabilized by different ligands.[3] In a series of pioneering papers, Weaver et al.[4] demonstrated that divalent europium can be stabilized with the famous 2:2:2 and 2:2:1 cryptands reported by Lehn.[5] These Eu^{2+} cryptates were shown later to present interesting photophysical properties, as in contrast to the aqua ion they show luminescence emission in aqueous solution even at room temperature.[6] More recently, the Eu^{2+} 2:2:2 cryptate was proposed as a synthon for potential pO_2 responsive contrast agents for magnetic resonance imaging (MRI).[7] Most of the commercially available contrast agents for MRI are Gd^{3+} complexes with polyaminocarboxylate ligands. The metal ion of choice is Gd^{3+} due to its high magnetic moment and symmetric ^8S electronic ground state associated with its $4f^7$ electron configuration, which results in relatively slow electron spin relaxation.[8] The Eu^{2+} ion is isoelectronic with Gd^{3+}, and thus efficiently enhances proton relaxation, while Eu^{3+} is a poor relaxation agent.

Different attempts to stabilize Eu^{2+} in aqueous media had limited success. The Eu^{2+} complex with the highest thermodynamic stability reported so far is $[Eu(dota)]^{2-}$ (log K = 16.75), but the redox stability of this complex and that of the 14-membered teta^{4-} ligand were found to be insufficient for potential use as an MRI contrast agent (Chart 1).[9] A similar situation holds for the Eu^{2+} complex with dtpa^{5-}.[10] The redox

Received: March 10, 2015
Published: May 5, 2015

DOI: 10.1021/acs.inorgchem.5b00548
Inorg. Chem. 2015, 54, 4940−4952

Chart 1. Chemical Structure of the Ligands Discussed in This Work

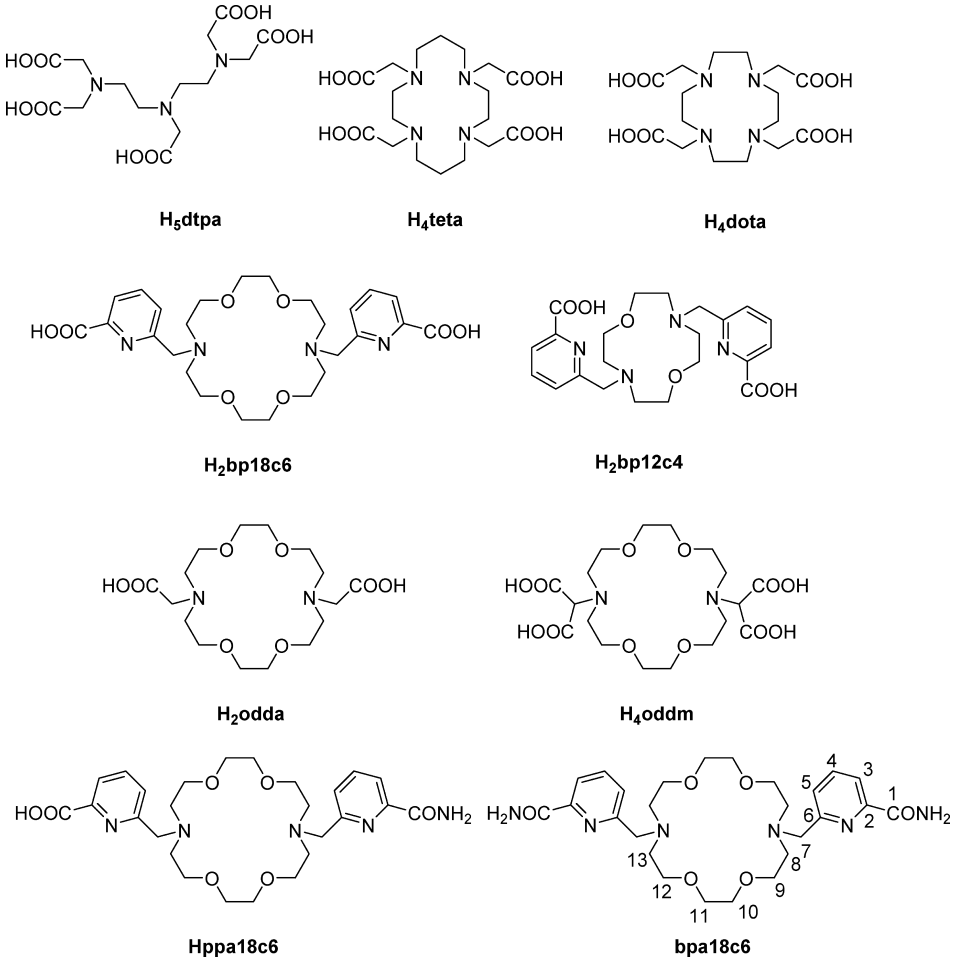

stability of the Eu^{2+} complexes is significantly higher when using 18-membered macrocyclic ligands such as H_4oddm and H_2odda.[11] A breakthrough in the coordination chemistry of Eu^{2+} in aqueous solution was achieved by Allen et al., who reported a series of oxidatively stable cryptates whose oxidation potentials were indicative of biological oxidative stability.[12] In subsequent works, it was shown that the kinetically inert $Eu(2{:}2{:}2)^{2+}$ cryptate[13] can be used as a oxidation responsive MRI contrast agent when encapsulated into liposomes,[14] or functionalized to target human serum albumin.[15]

In previous work we have shown that the $bp18c6^{2-}$ ligand provides an unprecedented selectivity for the large lanthanide ions ($\log K_{CeBP18C6} - \log K_{LuBP18C6} = 6.9$),[16] as well as a remarkable selectivity for Am^{3+} over Cm^{3+}, in spite of the small difference in ionic radii of these two adjacent actinide ions.[17] Thus, we hypothesized that the $bp18c6^{2-}$ ligand could stabilize to a certain extent the larger Eu^{2+} ion (ionic radius 1.25 Å for CN 8) over the smaller Eu^{3+} (ionic radius 1.066 Å for CN 8).[18] Indeed, the $bp18c6^{2-}$ ligand was also found to be very selective for Sr^{2+}, which has an ionic radius very similar to that of Eu^{2+}, over Ca^{2+} (ionic radius for CN 8, Sr^{2+} 1.26 Å; Ca^{2+} 1.12 Å).[19] Additionally, replacement of the hard carboxylate oxygen donor atoms of $bp18c6^{2-}$ by neutral amide oxygen atoms is expected to further stabilize the softer Eu^{2+} over the harder Eu^{3+} ion following the Pearson's HSAB principle.[20] Thus, in this contribution we report a comparative study of the ability of ligands $bp18c6^{2-}$, $ppa18c6^{-}$, and bpa18c6 to provide size-discrimination of the Ln^{3+} ions and stabilize Eu^{2+}.

RESULTS AND DISCUSSION

Synthesis and Characterization of the Ligands. Ligands Hppa18c6 and bpa18c6 were obtained by stirring the methyl ester derivative of H_2bp18c6[16] in concentrated aqueous ammonia at 0 °C. Under these conditions a mixture of both ligands was formed, which was separated using column chromatography. The bpa18c6 ligand was isolated in 43% yield, while the Hppa18c6 ligand was obtained as its K^+ complex in 50% yield.

Slow evaporation of an aqueous solution of bpa18c6 gave single crystals with formula bpa18c6·6H_2O suitable for X-ray diffraction analysis. This compound crystallizes in the monoclinic $P2_1/n$ space group, and the asymmetric unit contains a half ligand molecule and three water molecules (Figure 1). The pendant arms of the ligand are disposed in an *anti* conformation with respect to the macrocyclic fragment. The water molecules are involved in hydrogen-bonding interaction with the oxygen and nitrogen atoms of the azacrown moiety, as well as with the amide groups (Table S1, Supporting Information). The amide groups of neighbor molecules establish two symmetry related intermolecular hydrogen-bonds involving the *trans* hydrogen atom of the $-NH_2$ group and the carbonyl oxygen of an adjacent amide, producing an $R_2^2(8)$ motif typical of primary amides.[21]

DOI: 10.1021/acs.inorgchem.5b00548
Inorg. Chem. 2015, 54, 4940−4952

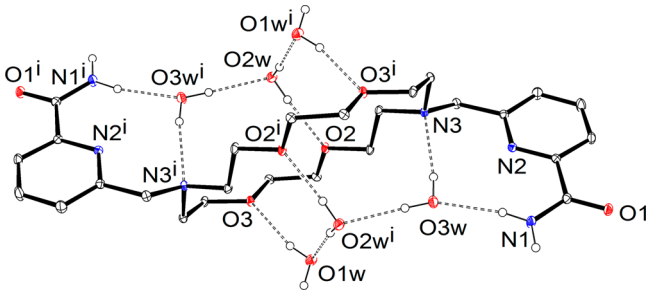

Figure 1. X-ray crystal structure of bpa18c6 with atom numbering. Hydrogen atoms, except those involved in hydrogen-bonds, are omitted for simplicity. The ORTEP plot is at the 30% probability level.

X-ray Structures of Metal Complexes. Single crystals with formula $[La(ppa18c6)(H_2O)](PF_6)_{1.44}(OTf)_{0.56}\cdot 2H_2O$ (Lappa18c6) were obtained by addition of KPF_6 to an aqueous solution of the complex, which was prepared by mixing stoichiometric amounts of the ligand and hydrated $La(OTf)_3$ in water at pH ~ 7.0. Crystals contain the $[La(ppa18c6)(H_2O)]^{2+}$ cation, two water molecules involved in hydrogen-bonds with the oxygen atom of the carboxylate group O8 and the coordinated water molecule, and heavily disordered TfO^- and PF_6^- anions. A view of the structure of the complex is shown in Figure 2, while bond distances of the metal coordination

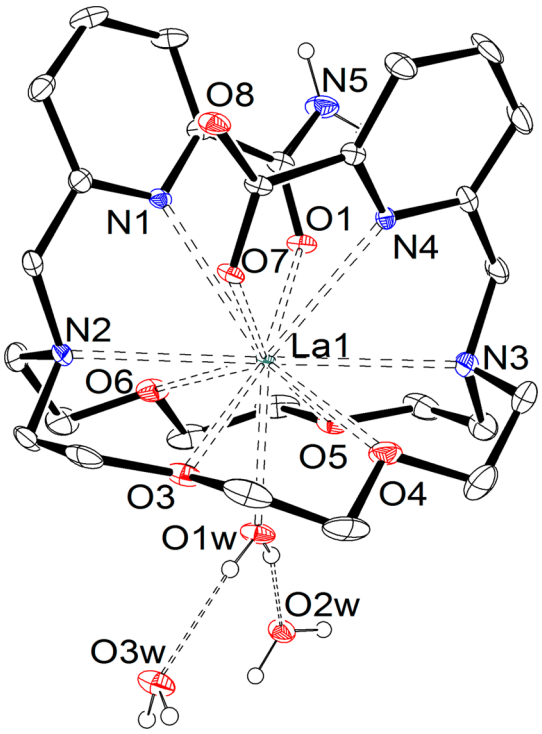

Figure 2. X-ray crystal structure of $[La(ppa18c6)(H_2O)](PF_6)_{1.44}(OTf)_{0.56}\cdot 2H_2O$ with atom numbering. Hydrogen atoms bonded to carbon atoms and anions are omitted for simplicity. The ORTEP plot is at the 30% probability level.

environment are given in Table 1. The La^{3+} ion is directly bound to the 10 donor atoms of the ligand, with 11-coordination being completed by an oxygen atom of a coordinated water molecule. The two pendant arms are located above the mean plane defined by the donor atoms of the azacrown moiety, which results in a *syn* conformation. The

Table 1. Bond Distances (Å) of the Metal Coordination Environments in $[La(ppa18c6)(H_2O)](PF_6)_{1.44}(OTf)_{0.56}\cdot 2H_2O$ and $[Sr(bpa18c6)(H_2O)](ClO_4)_2\cdot H_2O$

Lappa18c6		Srbpa18c6			
La1−O7	2.472(2)	Sr1−O(7	2.660(6)	Sr2−O9	2.658(7)
La1−O1w	2.511(2)	Sr1−O17	2.564(8)	Sr2−O18	2.692(8)
La1−O1	2.541(2)	Sr1−O1	2.675(6)	Sr2−O15	2.627(7)
La1−N4	2.731(3)	Sr1−N1	2.805(8)	Sr2−N5	2.801(7)
La1−O4	2.738(2)	Sr1−O4	2.779(6)	Sr2−O13	2.735(7)
La1−O6	2.765(2)	Sr1−O6	2.788(6)	Sr2−O12	2.752(6)
La1−O3	2.775(2)	Sr1−O3	2.792(6)	Sr2−O14	2.849(6)
La1−N1	2.777(3)	Sr1−N4	2.798(8)	Sr2−N8	2.844(8)
La1−O5	2.806(2)	Sr1−O5	2.825(5)	Sr2−O11	2.808(7)
La1−N2	2.891(3)	Sr1−N3	2.922(7)	Sr2−N7	2.957(8)
La1−N3	2.922(3)	Sr1−N2	2.910(8)	Sr2−N6	2.945(8)

bond distance involving the metal ion and the oxygen atom of the amide group (O1) is ca. 0.07 Å longer than the distance to the oxygen atom of the carboxylate group O7, which is in line with a stronger electrostatic interaction of the cation with the negatively charged picolinate group. The average distance between the La^{3+} ion and the oxygen atoms of the crown moiety (2.772 Å) is similar to that observed in the complex of the parent 1,4,10,13-tetraoxa-7,16-diazacyclooctadecane (18c6) ligand (2.769 Å),[22] in which three nitrate anions complete the metal coordination environment, and also close to that reported for the complex based on the same macrocyclic platform containing two 2-salicylaldiminobenzyl pendant arms (2.784 Å).[23] However, the average distance between the La^{3+} ion and the nitrogen atoms of the macrocyclic unit changes significantly depending upon the nature of the pendant arms. Indeed, this distance amounts to 2.731 Å in $[La(18c6)(NO_3)_3]$,[22] 2.908 Å in $[La(ppa18c6)(H_2O)]^{2+}$, and 3.023 Å in the complex with the ligand containing bulky 2-salicylaldiminobenzyl arms.[23] Thus, increasing the steric demand of the pendant arms attached to the macrocyclic unit weakens the interactions between the metal ion and the nitrogen atoms of the crown moiety. The rather short average La−N distance observed in the complex of $La(NCS)_3$ and dibenzyldiaza-18-crown-6 (2.800 Å), in which the pendant arms lack donor atoms for metal ion coordination, is in line with these observations.[24]

The coordinated water molecule in $[La(ppa18c6)(H_2O)]^{2+}$ is involved in a hydrogen-bonding interaction with the two noncoordinated water molecules present in the crystal lattice [O1w···O2w 2.722(3) Å, O1w−H12w···O2w 1.97(4) Å, O1w−H12w···O2w 166(4)°; O1w···O3w 2.730(4) Å, O1w−H1w···O3w 1.97(4) Å, O1w−H1w···O3w 160(4)°], which in turn are connected to PF_6^- anions and the oxygen atom of the carboxylate group O8. Similar hydrogen-bonding patterns involving a coordinated water molecule and two water molecules present in the crystal lattice have been observed previously.[25] Interestingly, we have also shown that the explicit inclusion of two second-sphere water molecules connected to the coordinated water molecule via hydrogen-bonds was crucial to compute accurate $Gd-O_{water}$ distances and ^{17}O hyperfine coupling constants.[26]

The *syn* conformation of the ligand in the $[La(ppa18c6)(H_2O)]^{2+}$ complex results in the presence of two different sources of chirality: One is associated with the layout of the two pendant groups (often represented as Δ or Λ), and the second one is related to the conformations of the six five-membered

DOI: 10.1021/acs.inorgchem.5b00548
Inorg. Chem. 2015, 54, 4940−4952

chelate rings formed upon coordination of the macrocyclic moiety.[27,28] Depending on the sign of the N−C−C−O and O−C−C−O torsion angles, the conformation of each five-membered chelate ring in the macrocyclic ligand can be left-handed, designed as λ (negative torsion angle), or right-handed, designed as δ (positive torsion angle). Inspection of the crystal data shows that in the case of $[La(ppa18c6)(H_2O)]^{2+}$ the enantiomeric forms $\Lambda(\lambda\delta\lambda)(\lambda\delta\lambda)$ and $\Delta(\delta\lambda\delta)(\delta\lambda\delta)$ are both present in the crystal lattice due to the centrosymmetric nature of the $P2_1/n$ monoclinic space group. Moreover, the crown moiety adopts the same conformation in $[La(18c6)(NO_3)_3]$[22] and in the complex of $La(NCS)_3$ and dibenzyldiaza-18-crown-6.[24]

Crystals of formula $[Sr(bpa18c6)(H_2O)](ClO_4)_2\cdot H_2O$ (Srbpa18c6) were obtained by slow evaporation of an aqueous solution (30 mM) containing equimolar amounts of the ligand and $Sr(ClO_4)_2$ at neutral pH. This compound crystallizes in the monoclinic $P2_1$ space group, and the asymmetric unit contains two $[Sr(bpa18c6)(H_2O)]^{2+}$ entities with different bond distances and angles of the metal coordination environment, four perchlorate anions, and water molecules. A view of the crystal structure is presented in Figure 3, while bond distances of the Sr^{2+} coordination environments are provided in Table 1. As observed for $[La(ppa18c6)(H_2O)]^{2+}$, the metal ion is directly coordinated to the 10 donor atoms of the ligand. The 11-coordination is completed by the presence of an inner-sphere water molecule. Coordination of the water molecule and the donor atoms of the pendant arms occurs from opposite sides of the crown moiety. A similar situation was observed in the solid state for the Sr^{2+} complex of D,L-7,16-bis(2-hydroxycyclohexyl)-1,4,10,13-tetraoxa-7,16-diazacyclooctadecane,[29] and assumed to occur in solution for [Sr(odda)] on the basis of the X-ray structure, which presents an oxygen atom of a neighbor [Sr(odda)] entity coordinated in the side of the macrocycle opposite to the carboxylate pendant arms.[11] The bond distances involving the 11-coordinated Sr^{2+} ion and the donor atoms of the crown moiety are longer than those observed in the nine-coordinate [Sr(odda)] complex[11] and other nine-coordinate Sr^{2+} complexes with ligands derived from the same crown moiety.[30] The $[Sr(bpa18c6)(H_2O)]^{2+}$ complex presents a $\Lambda(\lambda\delta\lambda)(\lambda\delta\lambda)$ conformation in the solid state, with only one enantiomer being present in the crystal lattice due to the chiral nature of the monoclinic $P2_1/n$ space group. The conformation adopted by the crown moiety is identical to that observed for $[La(ppa18c6)(H_2O)]^{2+}$ (see above) and related complexes with large metal ions such as $[Pb(bp18c6)]^{2+}$.[19] Thus, this particular conformation appears to be particularly well-suited for the coordination to large metal ions.

The two $[Sr(bpa18c6)(H_2O)]^{2+}$ entities present in the X-ray structure of Srbpa18c6 present rather different bond distances involving the metal ion and the oxygen atom of the coordinated water molecule: Sr1−O17, 2.564(8) Å, and Sr2−O18, 2.692(8) Å. A careful inspection of the crystal structure shows that the water molecule providing the strongest interaction with the Sr^{2+} ion establishes rather strong hydrogen-bonds with two oxygen atoms of two perchlorate anion [O17···O32 2.92(2) Å, O17−H172···O32 2.23(11) Å, O17−H172···O32 163(14)°; O17···O23 3.03(4) Å, O17−H171···O23 2.27(13) Å, O17−H171···O23 162(12)°]. On the other hand, the water molecule coordinated to Sr2 is establishing a weak hydrogen-bond with both an oxygen atom of a noncoordinated water molecule [O18···O1w 3.04(2) Å, O18−H182···O1w 2.40(8) Å, O18−H182···O1w 134(10)°] and an oxygen atom from a perchlorate ion [O18···O20 3.03(1) Å, O18−H181···O20 2.41 (9) Å, O18−H181···O20 131(10)°]. Thus, the stronger the hydrogen-bonds involving the coordinated water molecule and hydrogen-bond acceptors present in the crystal lattice are, the shorter the distances between the metal ion and the coordinated water molecule are. A similar effect has been reported in a theoretical investigation of uranyl complexes.[31] In that work, O−H···N hydrogen-bonds involving the coordinated water molecules and acetonitrile molecules in the second solvation shell were found to increase the dipole moment of the water ligand significantly, which reinforced the ionic part of the metal−water bond. The solid state structure of $[Sr(bpa18c6)(H_2O)]^{2+}$ appears to provide experimental evidence for this effect.

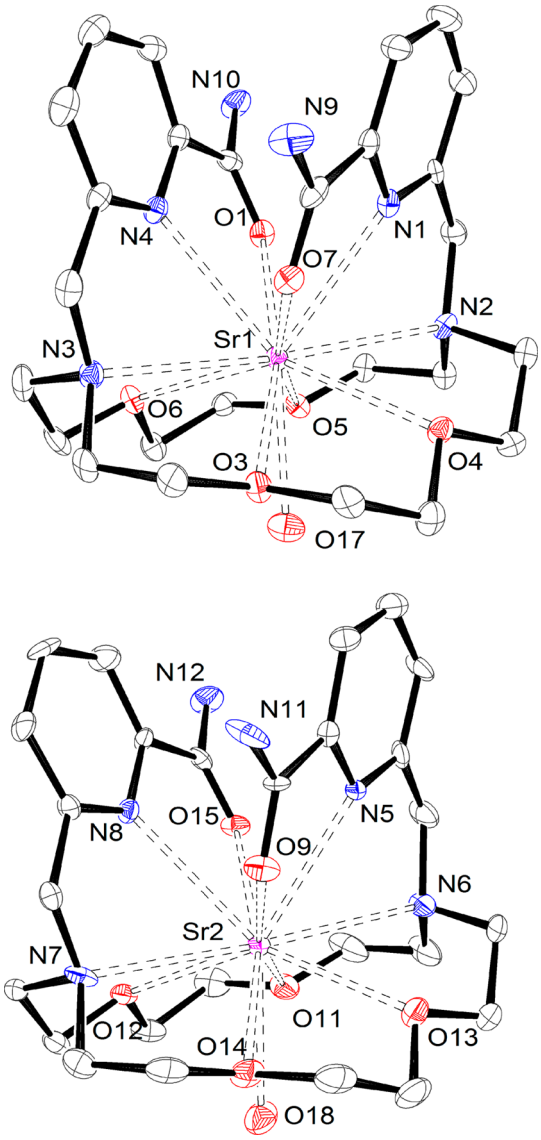

Figure 3. View of the two complex cations present in the asymmetric unit of crystals with formula $[Sr(bpa18c6)(H_2O)](ClO_4)_2\cdot H_2O$. Hydrogen atoms are omitted for simplicity. The ORTEP plots are at the 30% probability level.

Structures in Solution. The ESI^+ mass spectra recorded from aqueous solutions containing equimolar amounts of La^{3+} or Eu^{3+} and bpa18c6 or $ppa18c6^-$ at neutral pH show peaks due to the $[Ln(ppa18c6)]^{2+}$ or $[Ln(bpa18c6\text{-}H)]^{2+}$ entities, which confirm the formation of the expected 1:1 (Ln:ligand) complexes. The corresponding high-resolution spectra provided

DOI: 10.1021/acs.inorgchem.5b00548
Inorg. Chem. 2015, 54, 4940−4952

isotropic distributions for these peaks in nice agreement with the calculated ones, which is particularly evident in the case of the Eu^{3+} complexes with the presence of ^{151}Eu and ^{153}Eu isotopes (Figures S3−S7, Supporting Information).

The ^1H NMR spectra of the diamagnetic $[La(bpa18c6)]^{3+}$ complex recorded in D_2O solution presents 17 signals for the 38 proton nuclei of the ligand (the signals due to amide protons are not observed in D_2O), which points to a C_2 symmetry of the complex in solution. This is confirmed by the ^{13}C NMR spectrum, which shows 13 signals (Figure S8, Supporting Information). The diastereotopic nature of the proton signals of the macrocyclic unit and the methylenic protons of the pendant arms points to a rather rigid structure of the complex, and suggests that a single diastereoisomer is present in solution. A full attribution of the ^1H and ^{13}C signals was achieved with the aid of homonuclear $^1H-^1H$ COSY experiments and heteronuclear HSQC and HMBC experiments (Table 2). The assignment of the macrocyclic axial and

Table 2. ^1H and ^{13}C NMR Shifts (ppm with Respect to TMS) for $[Ln(bpa18c6)]^{3+}$ (Ln = La, Pr)[a]

	La[a]		La[a,b]	Pr, δ_i^{exp}	Pr, δ_i^{calcc}
C1	169.9	H3	7.46	16.26	14.29
C2	145.6	H4	7.87	11.66	10.79
C3	121.1	H5	7.58	6.76	6.57
C4	140.6	H7ax	3.54	−12.37	−10.55
C5	127.9	H7eq	4.92	−8.98	−9.47
C6	159.2	H8ax	2.70	−26.87	−24.27
C7	59.1	H8eq	2.29	−14.30	−16.08
C8	55.5	H9ax	3.99	−7.04	−6.12
C9	68.7	H9eq	3.35	−4.76	−6.04
C10	71.3	H10ax	3.99	19.18	23.29
C11	69.7	H10eq	3.50	8.52	7.35
C12	67.6	H11ax	3.87	9.39	10.65
C13	52.9	H11eq	3.56	11.66	10.70
		H12ax	4.26	−5.15	−3.43
		H12eq	3.69	3.00	0.96
		H13ax	3.42	−14.61	−13.12
		H13eq	2.46	−10.79	−12.42

[a]Assignment supported by 2D COSY, HSQC, and HMBC experiments in D_2O at 298 K and pD = 7.0. [b]$^3J_{3,4}$ = 7.8 Hz; $^3J_{5,4}$ = 7.9 Hz; $^2J_{7ax,7eq}$ = 16.5 Hz; $^2J_{8ax,8eq}$ = 14.0 Hz; $^2J_{9ax,9eq}$ = 10.8 Hz; $^2J_{10ax,10eq}$ = 10.4 Hz; $^2J_{11ax,11eq}$ = 10.2 Hz; $^2J_{12ax,12eq}$ = 10.5 Hz; $^2J_{13ax,13eq}$ = 14.0 Hz. [c]Calculated values obtained using eq 1 and the geometry of the $\Delta(\delta\lambda\delta)(\delta\lambda\delta)$ isomer optimized at the TPSSh/LCRECP/6-31G(d,p) level.

equatorial proton signals was achieved by analyzing their $^1H-^1H$ coupling patterns, as described previously.[32] The axial protons provide two strong couplings, the $^2J_{ax\text{-}eq}$ coupling (~16 Hz) and the $^2J_{ax\text{-}ax}$ coupling (~14 Hz), while equatorial protons give only one strong coupling ($^2J_{eq\text{-}ax}$). The ^{13}C NMR spectrum of $[La(ppa18c6)]^{2+}$ shows however 26 signals, which is in line with the C_1 symmetry expected due to the different nature of the pendant arms. The ^1H NMR spectrum also points to a very rigid structure in solution with the presence of only one diastereoisomer (Figure S9, Supporting Information). The ^1H NMR spectra of the paramagnetic $[Ln(ppa18c6)]^{2+}$ complexes (Ln = Pr, Eu, and Yb, 25 °C) are well-resolved; they consist of 34 paramagnetically shifted resonances observed in the range −33 to +36 ppm (Pr), −11 to +12 ppm (Eu), and −59 to +46 ppm (Yb). This suggests that these complexes exist as a single diastereoisomer in solution for the whole lanthanide series from La to Yb (Figures S10−S12, Supporting Information).

The ^1H NMR spectrum of a D_2O solution containing equimolar amounts of bpa18c6 and Yb^{3+} chloride (~20 mM, pD = 7.0) does not show paramagnetically shifted resonances, with signals due to the uncomplexed ligand only being observed. However, the spectra of the Pr^{3+} and Eu^{3+} complexes are well-resolved (Figure 4), although in the latter case some

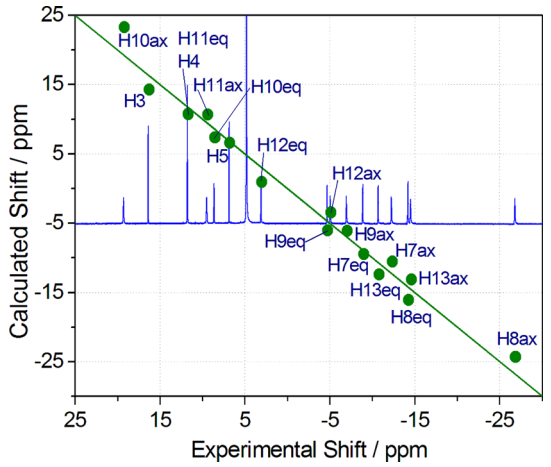

Figure 4. ^1H NMR (300 MHz, 298 K) spectrum of $[Pr(bpa18c6)]^{3+}$ recorded in D_2O solution (~30 mM, pH = 7.0) and plot of the experimental shifts versus those calculated with the DFT optimized geometry and pseudocontact contributions $[\Delta(\delta\lambda\delta)(\delta\lambda\delta)$ isomer]. The solid line represents a perfect fit between experimental and calculated values.

resonances are considerably broad (Figures S10−S11, Supporting Information). These results are in line with a decrease of the complex stability upon moving to the right across the lanthanide series (see stability constants reported below).

To gain information on the structure of the complexes in solution we performed DFT calculations at the TPSSh/LCRECP/6-31G(d,p) level. Our calculations and NMR studies reported previously for $[Ln(bp18c6)]^+$ showed that the complexes with the large Ln^{3+} ions present a $\Delta(\delta\lambda\delta)(\delta\lambda\delta)$ conformation in solution, where Δ represents the helicity associated with the layout of the two picolinate pendant arms, and symbols δ and λ refer to the conformations adopted by the six five-membered chelate rings formed due to the coordination of the macrocyclic moiety. A second conformation, $\Delta(\lambda\delta\lambda)$-$(\lambda\delta\lambda)$, also had a relatively low energy, particularly for the small Ln^{3+} ions. The relative stabilities of these two diastereomeric forms obtained with DFT calculations for the $[Ln(bpa18c6)]^{3+}$ and $[Ln(ppa18c6)]^{2+}$ systems reveal a similar picture (Figure S13, Supporting Information), with the $\Delta(\delta\lambda\delta)(\delta\lambda\delta)$ conformation being the most stable one along the whole 4f period. This is in line with the conformations observed in the X-ray crystal structures described above.

The structure of the $[Pr(bpa18c6)]^{3+}$ complex in solution was investigated by analyzing the Pr^{3+}-induced paramagnetic shifts.[33] The paramagnetic ^1H shifts induced by this metal ion are expected to be dominated by pseudocontact contributions,[34] which for the general case of nonaxial symmetry can be described by the following equation:[35]

DOI: 10.1021/acs.inorgchem.5b00548
Inorg. Chem. 2015, 54, 4940−4952

Table 3. Protonation Constants of bp18c6^{2-}, ppa18c6^{-}, and bpa18c6 (25 °C, 0.1 M KCl); Stability Constants of their Complexes with Ln^{3+} Ions; Half-Wave Potentials ($E_{1/2}$) of Eu^{3+}/Eu^{2+} Complexes; and Stability Constants of Eu^{2+} Complexes

	bpa18c6	ppa18c6^{-}	bp18c6^{2-a}	oddm^{4-b}	odda^{2-c}	bp12c4^{2-d}
log K_1^H	7.08(1)	7.13(1)	7.41	7.95	8.45	9.16
log K_2^H	6.40(1)	6.60(1)	6.85	7.35	7.80	7.54
log K_3^H		2.71(1)	3.32	3.03	2.90	3.76
log K_4^H			2.36			2.79
log K_{LaL}	8.63(2)	11.99(1)	14.99	*f*	12.21	16.81
log K_{CeL}	*f*	*f*		16.15		16.94
log K_{EuL}	5.17(6)	9.09(1)	13.01	*f*	12.02	18.62
log K_{GdL}	*f*	*f*	13.02	15.51	11.93	18.82
log K_{TbL}	*f*	7.76(1)	11.79	*f*	11.70	*f*
$E_{1/2}$/mV	−453	−610	−753	−920	−820	
log $K_{Eu^{2+}}$[e]	7.40	8.67	10.17	13.07	9.85	

[a]Reference 16. [b]Reference 38. [c]Reference 39. [d]Reference 40. [e]Calculated values from eq 4. [f]Not measured.

$$\delta_{ij}^{dip} = \left(\chi_{zz} - \frac{1}{3}\mathrm{tr}\,\chi\right)\left(\frac{3z^2 - r^2}{r^5}\right) + (\chi_{xx} - \chi_{yy})\left(\frac{x^2 - y^2}{r^5}\right) \quad (1)$$

Here, *x*, *y*, and *z* are the Cartesian coordinates of the observed nucleus with the Ln^{3+} at the origin, $[\chi_{zz} - {}^1/_3(\chi_{xx} + \chi_{yy} + \chi_{zz})]$ and $(\chi_{xx} - \chi_{yy})$ are the axial and rhombic anisotropies of the magnetic susceptibility tensor χ, respectively, and $r = (x^2 + y^2 + z^2)^{1/2}$. The analysis followed our previous works on complexes with C_2 symmetries, by taking the principal magnetic axis at the position of the C_2 symmetry axis of the molecule while allowing the position of the *x* and *y* magnetic axis in the perpendicular plane to vary.[33,36] The ^{1}H NMR chemical shifts observed for the La^{3+} complex were taken as diamagnetic reference.

The structures of the $\Delta(\delta\lambda\delta)(\delta\lambda\delta)$ and $\Delta(\lambda\delta\lambda)(\lambda\delta\lambda)$ isomers obtained with DFT optimization in aqueous solution were used to assess the agreement between the experimental and calculated shifts of $[Pr(bpa18c6)]^{3+}$. The $\Delta(\lambda\delta\lambda)(\lambda\delta\lambda)$ isomer provides poor agreement between experimental and calculated values ($AF_j = 0.275$), while a much better agreement was obtained for the $\Delta(\delta\lambda\delta)(\delta\lambda\delta)$ form ($AF_j = 0.140$).[37] In the latter case the differences between the experimental and calculated shifts are <2.05 ppm for all protons except H10ax, which deviates 4.1 ppm (Table 2, see also Figure 4). Furthermore, the agreement factor obtained is similar to those obtained for other Pr^{3+} complexes.[33] As expected for a nonaxial system, the calculated $\chi_{zz} - {}^1/_3$ tr χ and $\chi_{xx} - \chi_{yy}$ values (−828 ± 36 and −1165 ± 46 ppm Å^3, respectively) define a rhombic magnetic susceptibility tensor. A similar analysis performed using the optimized geometries of the $[Pr(bpa18c6)(H_2O)]^{3+}\cdot 2H_2O$ system provides virtually identical agreement factors and magnetic susceptibility tensor, which indicates that the presence of a coordinated water molecule does not significantly affect the folding of the ligand around the paramagnetic ion. Thus, these results unambiguously demonstrate that the $[Pr(bpa18c6)]^{3+}$ complex adopts a $\Delta(\delta\lambda\delta)(\delta\lambda\delta)$ conformation in solution, as shown previously for $[Pr(bp18c6)]^{+}$.[16] Thus, it is reasonable to assume that $[Pr(ppa18c6)]^{2+}$ presents a $\Delta(\delta\lambda\delta)(\delta\lambda\delta)$ conformation in solution as well. This is in agreement with the relative energies of the $\Delta(\delta\lambda\delta)(\delta\lambda\delta)$ and $\Delta(\lambda\delta\lambda)(\lambda\delta\lambda)$ isomers described above.

The longitudinal water proton relaxivity, r_1, has been measured in a 1.0 mM aqueous solution of the $[Gd(ppa18c6)]^{2+}$ complex at pH 7.4. At 20 MHz and 25 °C, the relaxivity is 1.52 mM^{-1} s^{-1} which clearly points to a pure outer-sphere relaxation effect, thus providing evidence for the absence of inner-sphere water. Therefore, due to the decreasing lanthanide size, the inner-sphere water is expelled on going from the La^{3+} complex (monohydration proved by the X-ray structure) to the Gd^{3+} analogue, at least in the solution state.

Ligand Protonation Constants and Stability Constants of the Ln^{3+} Complexes. The protonation constants of ppa18c6^{-} and bpa18c6 were measured by using the standard pH-potentiometric technique in 0.1 M KCl (Figures S14 and S15, Supporting Information). The ligand protonation constants are defined as in eq 2:

$$K_i^H = \frac{[H_iL]}{[H_{i-1}L][H^+]} \quad (2)$$

Two protonation constants could be determined from the potentiometric curves of bpa18c6, which correspond to the protonation of the nitrogen atoms of the macrocyclic unit. These protonation constants slightly increase as the negative charge of the ligand increases following the sequence bpa18c6 < ppa18c6^{-} < bp18c6^{2-}. For ppa18c6^{-} a third protonation constant (log K_3^H) could be determined, which corresponds to the protonation of the picolinate group of the ligand (Table 3).[41]

The stability constants of the complexes of ppa18c6^{-} and bpa18c6 with selected Ln^{3+} ions, expressed as in eq 3, have also been determined by pH potentiometry in 0.1 M KCl.

$$K_{ML} = \frac{[ML]}{[M][L]} \quad (3)$$

As expected, the stability of the Ln^{3+} complexes decreases upon substitution of the negatively charged carboxylate groups by charge neutral amide groups. Each substitution results in a stability drop of ca. 3 log *K* units for the La^{3+} complexes, and ∼4 log *K* units for the Eu^{3+} complexes. As a result, the size-discrimination ability of these series of ligands increases following the order bp18c6^{2-} < ppa18c6^{-} < bpa18c6. Indeed, the differences in stability constants of the La^{3+} and Eu^{3+} complexes are log K_{La} − log K_{Eu} = 1.98 (bp18c6^{2-}), 2.90 (ppa18c6^{-}), and 3.46 (bpa18c6). Unfortunately, the stability constants of the Lu^{3+} complexes of bpa18c6 and ppa18c6^{-} could not be determined from the potentiometric data, as their low stability resulted in the precipitation of hydroxide species. However, the stability constant of the Tb^{3+} complex of ppa18c6^{-} confirms the higher selectivity of the latter ligand for the large lanthanides compared with bp18c6^{2-}: logK_{La} − logK_{Tb} = 3.20 (bp18c6^{2-}) and 4.23 (ppa18c6^{-}).

DOI: 10.1021/acs.inorgchem.5b00548
Inorg. Chem. 2015, 54, 4940−4952

The size-discrimination ability of $bp18c6^{2-}$ has been related to a better fit of the donor atoms offered by the ligand and the large Ln^{3+} ions, which results in a weakening of some of the interactions between the metal ion and some donor atoms of the ligand as the ionic radius of the metal ion decreases.[16,42] Inspection of the bond distances of the metal coordination environment calculated for the $[Ln(bpa18c6)]^{3+}$ and $[Ln(ppa18c6)]^{2+}$ complexes along the lanthanide series reveals a similar situation (Figures S16 and S17, Supporting Information). Indeed, while most of the bond distances decrease along the lanthanide series as a consequence of the lanthanide contraction, the distances between the metal ion and the nitrogen atoms of the macrocyclic unit remain nearly constant along the series. Furthermore, the distances between the Ln^{3+} ion and two oxygen atoms of the crown moiety experience a limited contraction along the series (<0.12 Å) when compared to the diminution of the ionic radius from La^{3+} to Lu^{3+} (~0.18 Å).[18]

The evolution of the stability of $[Ln(bpa18c6)]^{3+}$ and $[Ln(ppa18c6)]^{2+}$ complexes in aqueous solution was further analyzed by using the thermodynamic cycle presented in Scheme 1, following the same procedure reported recently for the $[Ln(bp18c6)]^{+}$ complexes.[43]

Scheme 1. Thermodynamic Cycle Used for the Analysis of Complex Stabilities along the Lanthanide Series

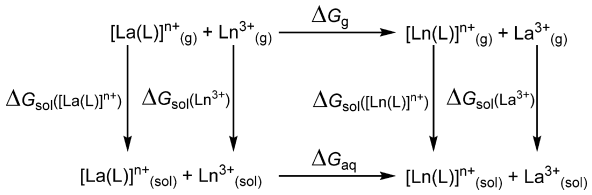

Our calculations show that ΔG_g values become more negative on proceeding to the right across the lanthanide series for the three series of complexes (Figure 5, see also Table 4), which is a consequence of the increased charge density of the metal ion. However, the calculated ΔG_g values obtained for the three series of complexes diverge along the lanthanide series, becoming more negative for the complexes of $bp18c6^{2-}$ than for those of $ppa18c6^{-}$ and bpa18c6. Thus, negatively charged ligands provide higher selectivities of the small Ln^{3+} ions in the gas phase as a consequence of the increased electrostatic interaction between the ligand and the metal ion.

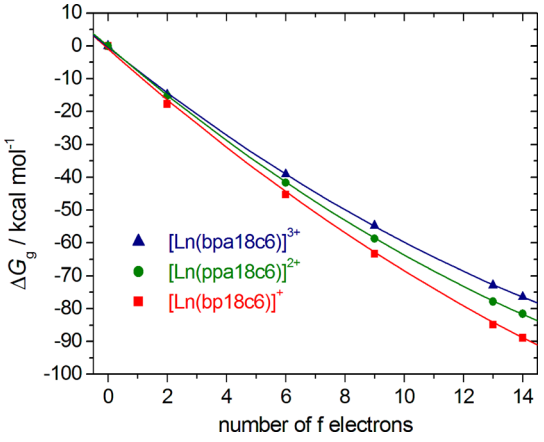

Figure 5. Gibbs free energies computed in the gas phase following Scheme 1 (ΔG_g values).

Table 4. Calculated Solvation Free Energies and Gibbs Free Energies (kcal mol^{-1}) in the Gas Phase (ΔG_g) and in Aqueous Solution (ΔG_{sol})[a]

	ΔG_g[a]	ΔG_{sol}(LnL)	ΔG_{aq}
		$bp18c6^{2-}$[b]	
La	0.00	−66.71	0.00
Pr	−17.67	−67.10	3.94
Eu	−45.24	−66.12	8.34
Dy	−63.33	−66.22	8.96
Yb	−84.86	−66.55	11.29
Lu	−88.89	−66.69	11.13
		$ppa18c6^{-}$	
La	0.00	−152.01	0.00
Pr	−15.14	−153.42	5.45
Eu	−41.61	−154.28	9.12
Dy	−58.73	−154.19	10.89
Yb	−77.85	−154.57	15.59
Lu	−81.61	−154.76	15.64
		bpa18c6	
La	0.00	−293.36	0.00
Pr	−14.81	−295.16	5.38
Eu	−39.06	−295.87	11.43
Dy	−54.71	−297.34	13.11
Yb	−72.92	−299.23	17.20
Lu	−76.40	−299.64	17.31

[a]BSSE corrections taken into account with the counterpoise method. [b]Values taken from ref 43.

The hydration free energies (Table 4) vary in the order $[Ln(bp18c6)]^{+}$ < $[Ln(ppa18c6)]^{2+}$ < $[Ln(bpa18c6)]^{3+}$, as expected considering the electric charge of the complexes. The complexes formed with a given ligand present similar structures along the lanthanide series, and therefore hydration free energies do not vary dramatically by changing the Ln^{3+} ion. The hydration free energies in $[Ln(bp18c6)]^{+}$ complexes differ by <1.0 kcal mol^{-1} across the series, while for $[Ln(ppa18c6)]^{2+}$ complexes they differ by less than 2.6 kcal mol^{-1}. However, the higher positive charge of the $[Ln(bpa18c6)]^{3+}$ complexes results in a smooth increase of the hydration free energies across the series that change by ca. 6.3 kcal mol^{-1} from La^{3+} to Lu^{3+}.

The Gibbs free energies calculated for the three series of complexes according to Scheme 1 take positive values that increase along the lanthanide series, in line with the stability trend given by the stability constants (Figure 6 and Table 4). The stability trends observed across the 4f period are mainly the result of a balance between two opposite factors: (i) The increasing hydration free energies of the Ln^{3+} ions across the series; (ii) the increasing binding energy of the ligand to the Ln^{3+} ions as their ionic radius decreases, which is reflected in the calculated ΔG_g values. For most lanthanide complexes this increasing binding energy overcomes the hydration energies of the Ln^{3+} ions, which results in increasing complex stabilities across the series.[43] In some instances these two factors cancel each other, resulting in complex stabilities that do not change significantly along the series.[42] Finally, in the systems investigated here the increasingly negative ΔG_g values do not compensate for the increasing hydration energies of the Ln^{3+} ions, resulting in reversal of the usual order of complex stability. The selectivity for the large Ln^{3+} ions over the smaller ones

DOI: 10.1021/acs.inorgchem.5b00548
Inorg. Chem. 2015, 54, 4940−4952

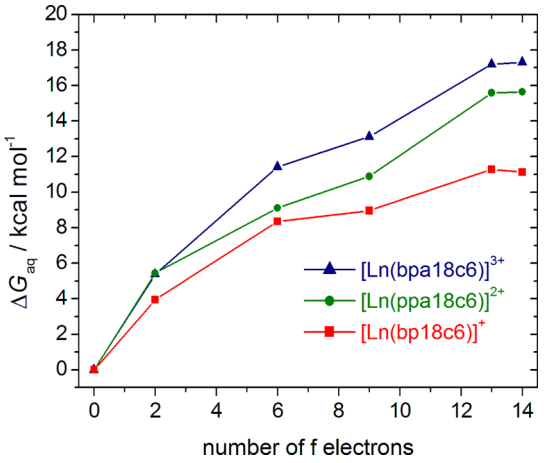

Figure 6. Gibbs free energies computed in aqueous solution following Scheme 1 (ΔG_{aq} values).

increases following the sequence bp18c6^{2-} < ppa18c6^{-} < bpa18c6, reflecting the variations observed for the ΔG_g values (Figure 5). This is in agreement with the stability constants determined for the La^{3+} and Eu^{3+} complexes (see above).

Stability of the Eu^{2+} Complexes. The redox stability of the Eu^{2+} complexes of bpa18c6, ppa18c6^{-}, and bp18c6^{2-} was evaluated by using cyclic voltammetry experiments in aqueous 0.1 M KCl. The cyclovoltammetric curves (Figure 7) are

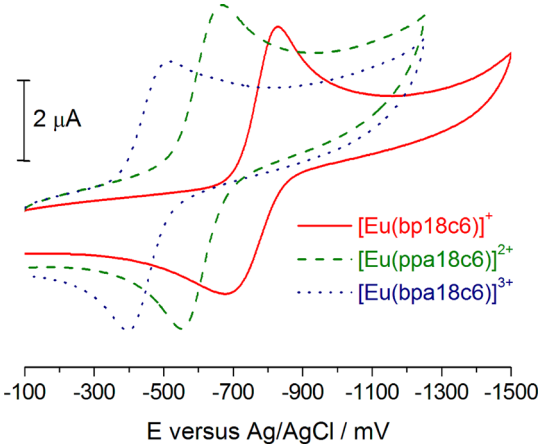

Figure 7. Cyclovoltammograms of Eu^{3+} complexes with diaza-18-crown-6 derivatives recorded from ca. 1 mM aqueous solutions (0.1 M KCl, pH 7.0, scan rates 0.05 V s^{-1}). The solutions of [Eu(bp18c6)]$^{+}$ and [Eu(ppa18c6)]$^{2+}$ contained a 10% ligand excess, while for [Eu(bpa18c6)]$^{3+}$ a 60% ligand excess was used to ensure full complexation of the metal ion.

characteristic of quasireversible systems with half-wave potentials of −753 mV (ΔE_p = 140 mV), −610 mV (ΔE_p = 110 mV), and −453 mV (ΔE_p = 115 mV) versus Ag/AgCl for bp18c6^{2-}, ppa18c6^{-}, and bpa18c6, respectively. These values reveal that the complexes of bp18c6^{2-} and ppa18c6^{-} possess lower stability against oxidation than the aquated ion, for which an $E_{1/2}$ value of −585 mV has been reported.[9] However, the $E_{1/2}$ value measured for the complex with bpa18c6 indicates higher redox stability than the aquated ion. Table 3 compares the half-wave potentials measured for these complexes with those reported previously for the complexes with oddm^{4-} and odda^{2-}. The latter two complexes show more negative $E_{1/2}$ values, which reflect their lower resistance to oxidation. This is not surprising considering that both oddm^{4-} and odda^{2-} present lower size-discrimination ability, as reflected by the stability constants determined for the Ln^{3+} complexes across the 4f period.[38,39] Additionally, the values reported in Table 3 clearly show that increasing the negative charge of the ligand is detrimental to the redox stability of the corresponding Eu^{2+} complexes. To assess the effect of the size of the macrocyclic cavity on Eu^{2+} stabilization we have also performed cyclic voltammetry experiments for the complex of bp12c4^{2-}, which contains a 12-membered macrocycle (Figure S18, Supporting Information).[44] The cyclovoltammogram recorded for this complex has clearly different current intensities for the widely separated anodic and cathodic peaks, which reflects an irreversible process. However, the cathodic peak potential (−1064 mV) is clearly more negative than that observed for the complex of bp18c6^{2-} (−828 mV), which shows that the presence of a 12-membered macrocycle is unfavorable for the stabilization of the large Eu^{2+} ion.

Following previous studies,[45] the thermodynamic stabilities of the Eu^{2+} complexes were evaluated by using the following relationship (Table 3):

$$\Delta E_{1/2} = E_{1/2,\text{complex}} - E_{1/2,\text{Eu}_{aq}} = \frac{RT}{F}\ln\frac{K_{Eu^{2+}}}{K_{Eu^{3+}}} \quad (4)$$

Here, $K_{Eu^{2+}}$ and $K_{Eu^{3+}}$ refer to the thermodynamic stability constants of the complex of divalent and trivalent europium, respectively. The stability constants of the Eu^{2+} complexes decrease upon replacing picolinate groups by neutral picolylamide units, in line with a decrease of the electrostatic interaction between the ligand and the metal ion. However, the diminution in complex stability is not as pronounced as for the corresponding Eu^{3+} complexes, which results in a remarkable stabilization of Eu^{2+} by the neutral bpa18c6 ligand. As observed for other macrocyclic and nonmacrocyclic ligands,[9] the stability constant obtained for the Eu^{2+} complex of bp18c6^{2-} (log $K_{Eu^{2+}}$ = 10.17) is slightly higher than that determined potentiometrically for the corresponding Sr^{2+} complex (log $K_{Sr^{2+}}$ = 9.57).[19]

The stabilities of the Eu^{2+} complexes were rationalized using the thermodynamic cycle shown in Scheme 2. The main results

Scheme 2. Thermodynamic Cycle Used for the Analysis of the Stabilities of Eu^{2+} Complexes

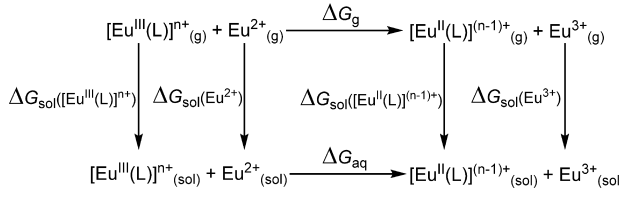

are given in Table 5. Our calculations provide positive ΔG_g values, as a consequence of the stronger electrostatic interaction between the ligands and the Eu^{3+} ion. The ΔG_g values are however reduced on decreasing the negative charge of the ligand, which shows that increasing the negative charge of the ligand is detrimental for the stabilization of the complexes with Eu^{2+}. Regarding the hydration free energies of the metal complexes, they become more negative upon increasing their positive electric charge. As a result, the smallest hydration free energy was calculated for the charge neutral [Eu^{II}(bp18c6)] complex.

DOI: 10.1021/acs.inorgchem.5b00548
Inorg. Chem. 2015, 54, 4940−4952

Table 5. Gibbs Free Energies and Solvation Free Energies (kcal mol^{-1}) Calculated According to Scheme 2

	bp18c6^{2-}	ppa18c6^{-}	bpa18c6[a]	bpa18c6[b]
ΔG_g	464.27	395.64	322.51	335.70
$\Delta G_{sol(Eu^{III}(L))^{n+}}$	−66.12	−154.28	−295.87	−286.45
$\Delta G_{sol(Eu^{II}(L))^{(n-1)+}}$	−34.18	−57.23	−132.92	−134.41
ΔG_{aq}	6.24	2.70	−4.52	−2.24
ΔG_{aq}(exptl)	3.87	0.57	−3.04	−3.04

[a]Results obtained for the $[Eu^{III}(bpa18c6)]^{3+}$ and $[Eu^{II}(bpa18c6)]^{2+}$ systems. [b]Results obtained for the $[Eu^{III}(bpa18c6)(H_2O)]^{3+}$ and $[Eu^{II}(bpa18c6)(H_2O)]^{2+}$ systems.

The Gibbs free energies in aqueous solution (ΔG_{aq}) were computed according to Scheme 2 as follows:

$$\Delta G_{aq} = \Delta G_g + \Delta G_{sol(Eu^{II}(L))^{(n-1)+}} + \Delta G_{sol(Eu^{3+})} - \Delta G_{sol(Eu^{III}(L))^{n+}} - \Delta G_{sol(Eu^{2+})} \quad (5)$$

The calculated ΔG_{aq} values reproduce fairly well the experimental trend obtained from the stability constants of the Eu^{3+} and Eu^{2+} complexes, with deviations <2.4 kcal mol^{-1}. The inclusion of a coordinated water molecule in the complexes of bpa18c6 has a minor effect in the calculated ΔG_{aq} values (~2.3 kcal mol^{-1}, Table 5).

The hydration free energies calculated for the Eu^{2+} complexes are in all cases less negative than the corresponding values for the complexes of Eu^{3+}. Thus, the relative values of the $\Delta G_{sol(Eu^{II}(L))^{(n-1)}}$ and $\Delta G_{sol(Eu^{III}(L))^{n+}}$ terms are not responsible for the huge stabilization of the Eu^{2+} complexes in aqueous solution with respect to the gas phase. The key factor for the stabilization of the Eu^{2+} complexes in solution is the higher hydration free energy of the trivalent Eu^{3+} ion compared to that of divalent Eu^{2+} (−841.1 and −354.2 kcal mol^{-1},[46,47] respectively, with the absolute hydration free energy of the H^+ ion equal to −264.0 kcal mol^{-1}).[48] The trend calculated for the ΔG_{aq} values is the result of the decrease of ΔG_g following the order bp18c6^{2-} > ppa18c6^{-} > bpa18c6, which compensates for an unfavorable balance of the hydration free energies, which amount to $\Delta G_{sol(Eu^{II}(L))^{(n-1)}} - \Delta G_{sol(Eu^{III}(L))^{n+}}$ = +31.95, +97.05, and +152.05 kcal mol^{-1} for L = bp18c6^{2-}, ppa18c6^{-}, and bpa18c6, respectively.

CONCLUSIONS

A detailed characterization of the structure of $[Ln(ppa18c6)]^{2+}$ and $[Ln(bpa18c6)]^{3+}$ complexes using X-ray crystallography, NMR spectroscopy, and DFT calculations shows that these complexes adopt $\Delta(\delta\lambda\delta)(\delta\lambda\delta)$ conformations in solution and in the solid state. The substitution of picolinate pendant arms of the ligand by charge neutral picolinamide groups decreases the stability of the metal complexes both with the Ln^{3+} ions and Eu^{2+} due to the reduced electrostatic interaction between the metal ion and the ligand. However, the charge neutral ligand bpa18c6 shows an enhanced size-discrimination ability compared to the parent anionic bp18c6^{2-} ligand, which could be exploited for the separation of Ln^{3+} ions using solvent extraction techniques. Our results also show that charge neutral ligands provide an important stabilization of Eu^{2+} with respect to their anionic counterparts. Furthermore, we have developed a computational approach for estimating the relative stability of Eu^{3+} and Eu^{2+} complexes, which will be helpful for the design of new ligands with increasing Eu^{2+} stabilization ability. Finally, the redox potentials determined for the $[Eu(bpa18c6)]^{3+}$ complex (−453 mV versus Ag/AgCl) lie slightly out of the range for typical biological oxidants and reductants (from −0.5 to +1.0 V versus NHE,[49] which corresponds to ca. −0.3 to 1.2 V versus Ag/AgCl 3 M KCl).[50] Thus, further optimization of divalent Eu^{2+} is still required for the design of Eu^{2+}-based redox-activated MRI contrast agents, which must also present high kinetic inertness to avoid metal ion release in vivo.

EXPERIMENTAL AND COMPUTATIONAL SECTION

Chemicals and Starting Materials. Chemicals were purchased from commercial sources and used without further purification. Dimethyl 6,6′-((1,4,10,13-tetraoxa-7,16-diazacyclooctadecane-7,16-diyl)bis(methylene))dipicolinate (**1**), H_2bp18c6, and H_2bp12c4 were prepared from the published procedures.[16,44] SiO_2 (Fluka, pore size 60 Å, 70−230 mesh) was used for preparative column chromatography. ^{1}H and ^{13}C NMR spectra were recorded at 25 °C on a Bruker Avance 300 or Bruker Avance 500 spectrometer. Samples of the Ln^{3+} complexes for the NMR measurements were prepared by dissolving equimolar amounts of the corresponding ligand and hydrated $Ln(OTf)_3$ in D_2O, followed by adjustment of the pD to ~7.0 with solutions of ND_4OD and DCl in D_2O. The final concentration of the complex was ca. 30 mM. ESI-TOF mass spectra were recorded using a LC-Q-q-TOF Applied Biosystems QSTAR Elite spectrometer in the positive mode. Aqueous solutions of the complexes for mass spectral analyses were prepared as described for NMR measurements using nondeuterated solvents. Elemental analyses were carried out on a ThermoQuest Flash EA 1112 elemental analyzer. IR spectra were recorded using a Bruker Vector 22 spectrophotometer equipped with a Golden Gate attenuated total reflectance (ATR) accessory (Specac).

Potentiometric Measurements. Carbonate-free 0.1 mol L^{-1} KOH and 0.1 mol L^{-1} HCl were prepared from Fisher Chemicals concentrates. Potentiometric titrations were performed in 0.1 mol L^{-1} aqueous KCl under nitrogen atmosphere, and the temperature was controlled to 25.0 ± 0.1 °C with a circulating water bath. The p[H] (p[H] = −log[H$^+$], concentration in molarity) was measured in each titration with a combined pH glass electrode (Metrohm) filled with 3 M KCl, and the titrant addition was automated by use of a 702 SM titrino system (Metrohm). The electrode was calibrated in hydrogen ion concentration by titration of HCl with KOH in 0.1 mol L^{-1} electrolyte solution.[51] A plot of meter reading versus p[H] allows the determination of the electrode standard potential ($E°$) and the slope factor (f). Continuous potentiometric titrations with HCl and KOH 0.1 mol L^{-1} were conducted on aqueous solutions containing 5 mL of Hppa18c6 2.52 mM and bpa18c6 2.51 mM in KCl 0.1 mol L^{-1}, with 2 min waiting between successive points. The titrations of the metal complexes were performed with the same ligand solutions containing 1 equiv of metal cation, with 2 min waiting time between 2 points. In the case of metal complexes only data corresponding to the lower portions of the titration curves were employed (pH < 5.0−5.6) to avoid complications arising from hydrolysis at higher pH values. However, inclusion of hydroxospecies in the model did not change significantly the calculated stability constants. Experimental data were refined using the computer program Hyperquad 2008.[52] All equilibrium constants are concentration quotients rather than activities and are defined as

$$K_{mlh} = \frac{[M_mL_lH_h]}{[M]^m[L]^l[H]^h} \quad (6)$$

The ionic product of water at 25 °C and 0.1 mol L^{-1} ionic strength is pK_w = 13.77.[53] Fixed values were used for pK_w; ligand acidity constants; and total concentrations of metal, ligand, and acid. All values and errors (one standard deviation) reported are at least the average of three independent experiments.

Cyclic Voltammetry. Cyclic voltammograms were recorded using a 797 VA Computrace potentiostat/galvanostat from Metrohm (Herisau, Switzerland) using a typical three electrode cell. A glassy carbon rotating disk electrode (RDE) was used as working electrode. The counter electrode was a platinum rod electrode. Potentials were measured using a Ag/AgCl reference electrode filled with 3 mol L^{-1}

DOI: 10.1021/acs.inorgchem.5b00548
Inorg. Chem. 2015, 54, 4940−4952

Table 6. Crystal Data and Refinement Details

	bpa18c6·6H_2O	Lappa18c6	Srbpa18c6
formula	$C_{26}H_{50}N_6O_{12}$	$C_{26.56}H_{42}F_{10.32}LaN_5O_{11.68}P_{1.44}S_{0.56}$	$C_{26}H_{42}Cl_2N_6O_{16}Sr$
CCDC number	1053031	1053030	1053029
MW	638.72	1015.79	853.17
cryst syst	monoclinic	monoclinic	monoclinic
space group	$P2_1/n$	$P2_1/c$	$P2_1$
T/K	100(2)	100(2)	100(2)
a/Å	13.446(1)	22.0177(12)	11.6607(3)
b/Å	8.155(1)	16.2990(8)	14.5010(4)
c/Å	15.9150(1)	10.5443(5)	21.2628(5)
α/deg	90	90	90
β/deg	112.728(4)	97.551(2)	99.4110(10)
γ/deg	90	90	90
V/Å^3	1609.6(3)	3751.2(3)	3546.97(16)
F(000)	688	2040.9	1760
Z	2	4	4
λ, Å (Mo Kα)	0.71073	0.71073	0.71073
D_{calc}/g cm^{-3}	1.318	1.797	1.598
μ/mm^{-1}	0.104	1.346	1.750
θ range/deg	1.69−26.43	1.559−26.372	1.707−25.350
R_{int}	0.0382	0.0712	0.0750
reflns measd	26 165	53 699	46 200
unique reflns	3308	7666	12 980
reflns obsd	2594	5863	9425
Flack parameter			0.004(8)
GOF on F^2	1.033	1.034	1.022
R1[a]	0.0386	0.0345	0.0567
wR2[b] (all data)	0.0923	0.0626	0.1144
largest differences peak and hole/e Å^{-3}	0.386/−0.294	0.798/−0.796	0.877/−0.554

[a] $R1 = \sum||F_o| - |F_c||/\sum|F_o|$. [b] $wR2 = \{\sum[w(|F_o|^2 - |F_c|^2)^2]/\sum[w(F_o^4)]\}^{1/2}$.

KCl. A stirring rate of 2000 rpm was used in the RDE. Solutions were purged with high purity (99.999%) nitrogen during 30 s prior recording the voltammograms. The starting and end potentials were −0.1 V, while the first vertex potential was set to −1.50 or −1.25 V depending on the potentials of the cathodic peaks. A sweep rate of 0.05 V s^{-1} was used in all the experiments. Solutions of the complexes for cyclic voltammetry measurements were prepared by mixing hydrated $EuCl_3$ and the ligand in aqueous 0.1 M KCl, followed by adjustment of the pH to 7.0 with aqueous KOH. A 10% ligand excess was used in all cases except $[Eu(bpa18c6)]^{3+}$, for which a 60% ligand excess was used to ensure full complexation of the metal ion (>97% as calculated with the equilibrium constants reported in Table 3).

Relaxivity Measurement. The water proton relaxivity was measured at 20 MHz and 25 °C for $[Gd(ppa18c6)]^{2+}$ at 1 mM concentration on a Bruker WP80 NMR electromagnet adapted to variable field measurements (20−80 MHz) and controlled by a Stelar SMARTracer PC-NMR console. The complex was prepared by dissolution of appropriate amounts of the ligand and hydrated $GdCl_3$ in H_2O, followed by adjustment of the pH to 7.0 with a diluted NaOH solution. A slight ligand excess (10%) was used to ensure full complexation of the metal ion (Figure S21, Supporting Information). The temperature was monitored by a VTC91 temperature control unit and maintained by a gas flow.

6,6′-((1,4,10,13-Tetraoxa-7,16-diazacyclooctadecane-7,16-diyl)bis(methylene))dipicolinamide (bpa18c6) and 6-((16-((6-Carbamoylpyridin-2-yl)methyl)-1,4,10,13-tetraoxa-7,16-diazacyclooctadecan-7-yl)methyl) Picolinate Potassium Salt (K(ppa18c6)). The ester precursor **1**·CH_2Cl_2 (1.00 g, 1.55 mmol) was stirred at 0 °C in concentrated aqueous ammonia (30 mL) for 4 h. Once the ester was completely dissolved, a second portion of aqueous ammonia (20 mL) was added, and the mixture was stored in the freezer for 16 h. The aqueous phase was extracted with CH_2Cl_2 (5 × 100 mL), and the organic phase was evaporated to dryness to give an oily residue that was purified by column chromatography on SiO_2 with a CH_3CN/H_2O/saturated aqueous KNO_3 mixture as eluent (14:3:x) using a gradient of saturated aqueous KNO_3 (x = 0−1). The fractions containing the two ligands were concentrated separately to eliminate the acetonitrile, and the resulting aqueous solutions (pH ∼ 8) were extracted with CH_2Cl_2 (5 × 100 mL). Evaporation of the organic extracts gave bpa18c6 and K(ppa18c6) as light yellow solids.

bpa18c6. Yield: 0.350 g, 43%. Anal. Calcd for $C_{26}H_{38}N_6O_6$: C 58.85, H 7.22, N 15.84%. Found: C 58.65, H 6.98, N 15.76%. MS (ESI$^+$, MeOH): m/z 531 ($[C_{26}H_{39}N_6O_6]^+$). IR (ATR): ν 1679 (C═O), 1591 and 1570 cm^{-1} (C═C), (C═N). ^{1}H NMR ($CDCl_3$, 500 MHz, 25 °C, TMS): δ 8.06 (d, 2H, ^3J = 7.7 Hz), 7.99 (s, 2H), 7.80 (t, 2H), 7.68 (d, 2H, ^3J = 7.7 Hz), 5.74 (s, 2H), 3.89 (s, 4H), 3.64 (m, 8H), 3.60 (s, 8H), 2.89 ppm (m, 8H). ^{13}C NMR ($CDCl_3$, 125.8 MHz, 25 °C, TMS): δ 166.9, 159.3, 148.7, 137.7, 125.8, 120.7, 70.7, 69.9, 61.3, 54.4 ppm.

K(ppa18c6)·KCl. Yield: 0.501 g, 50%. Anal. Calcd for $C_{26}H_{36}KN_5O_7$·KCl: C 48.47, H 5.63, N 10.87%. Found: C 48.99, H 5.97, N 10.42%. MS (ESI$^+$, MeOH): m/z 570 ($[C_{26}H_{37}KN_5O_7]^+$). IR (ATR): ν 1682 and 1613 (C═O), 1581 and 1570 cm^{-1} (C═C), (C═N). ^{1}H NMR ($CDCl_3$, 500 MHz, 25 °C, TMS): δ 8.85 (s, 1H), 8.03 (d, 1H, ^3J = 7.5 Hz), 7.84 (d, 1H, ^3J = 6.6 Hz), 7.71 (t, 1H), 7.61 (t, 1H), 7.40 (d, 1H, ^3J = 6.6 Hz), 7.10 (d, 1H, ^3J = 7.5 Hz), 5.97 (s, 1H), 3.99−2.56 ppm (m, 28H). ^{13}C NMR ($CDCl_3$, 125.8 MHz, 25 °C, TMS): δ 169.3, 167.5, 158.5, 156.4, 156.1, 149.6, 137.3, 136.9, 126.5, 123.5, 123.2, 120.3, 69.5, 69.3, 68.1, 67.7, 61.2, 59.8, 55.0, 54.7 ppm.

X-ray Diffraction Measurements. Three-dimensional X-ray data were collected on a Bruker Kappa APEXII CCD diffractometer. Data were corrected for Lorentz and polarization effects and for absorption by semiempirical methods[54] based on symmetry-equivalent reflections. Complex scattering factors were taken from the program SHELX2013[55] operating under the WinGX program system[56] as implemented on a Pentium computer. The structures were solved by

DOI: 10.1021/acs.inorgchem.5b00548
Inorg. Chem. 2015, 54, 4940−4952

direct methods using SIR2011[57] (bpa18c6·6H_2O) and SHELXS-2013[55] (Lappa18c6), or by Patterson methods with DIRDIF2008[58] (Srbpa18c6), and refined[55] by full-matrix least-squares on F^2. All hydrogen atoms were included in calculated positions and refined in riding mode in the three compounds, except those of the water molecules present in all three crystals that were located in a difference electron-density map and treated as follows: The usual DFIX (0.84(2)) and DANG (1.34(4)) restrictions were imposed for the three water molecules present in the asymmetric unit of bpa18c6·6H_2O. Crystals of Lappa18c6 contain three water molecules in the asymmetric unit, one coordinated to the metal ion and two noncoordinated; all atoms of these water molecules were refined freely, except those bonded to the noncoordinated oxygen atom O3W, for which O−H distances were restrained. Crystals of Srbpa18c6 contain four water molecules in the asymmetric unit, two of them not coordinated and disordered in five positions with occupation factors of 0.73, 0.39, 0.37, 0.26, and 0.25. These occupation factors and all the positional parameters were fixed during the refinement in order to reach convergence, except those of O18 and O3W, for which the usual DFIX (0.84(2)) and DANG (1.34(4)) restrictions where applied, and O17, for which the positions of the hydrogen atoms were refined freely. Moreover, for O4W an isotropic U_{ij} restraint was imposed in order to reach final convergence. Refinement converged with anisotropic displacement parameters for all non-hydrogen atoms. The anions are disordered in the crystals of both complexes; those of Lappa18c6 contain a PF_6^- anion having positional disorder with two positions for each fluorine atom with occupation factor of 0.79(2) for positions labeled with A and 0.21(2) for positions labeled with B. An isotropical restraint for the anisotropic displacement parameter U_{ij} of every fluorine atom in the group had to be imposed to reach final convergence. Crystals of Lappa18c6 also contain a $CF_3SO_3^-$ anion (occupation factor 0.559(6)) and a PF_6^- anion (occupation factor 0.441(6)) sharing the same site, so that 117 least-squares restraints were imposed to reach convergence. Two of the four perchlorate anions present in the asymmetric unit of the Srbpa18c6 crystal show positional disorder with occupation factors of 0.587(8) for Cl2 and the oxygen atoms bonded to it (0.413(8) for atoms labeled with B) and 0.590(9) for atoms of the perchlorate group including Cl4 (0.410(9) for atoms labeled with B). A total of 137 least-squares restraints were imposed to reach convergence. Crystal data and details on data collection and refinement are summarized in Table 6.

Computational Details. All calculations presented in this work were performed employing the Gaussian 09 package (Revision D.01).[59] Full geometry optimizations of the $[Ln(ppa18c6)]^{2+}$, $[Ln(bpa18c6)]^{3+}$, and $[Ln(bpa18c6)(H_2O)]^{3+}\cdot 2H_2O$ systems (Ln = La, Pr, Eu, Gd, Dy, Ho, Yb, or Lu) were done employing DFT within the hybrid meta generalized gradient approximation (hybrid meta-GGA), with the TPSSh exchange-correlation functional.[60] Geometry optimizations were carried out by using the large-core quasirelativistic effective core potential (LCRECP) of Dolg et al. and its associated [5s4p3d]-GTO valence basis set,[61] while the ligand atoms were described by using the standard 6-31G(d,p) basis set. Input geometries were taken from our previous computational studies.[16,43] Geometry optimizations of the complexes with divalent europium ($[Eu^{II}(bp18c6)]$, $[Eu^{II}(ppa18c6)]^+$, and $[Eu^{II}(bpa18c6)]^{2+}$) were performed using the same methodology. However, it is important to note that the use of LCRECPs, which include the 4f electrons in the core, requires a separate potential for each oxidation state or 4f subconfiguration, and therefore different ECPs were used for Eu^{3+} and Eu^{2+} complexes. No symmetry constraints have been imposed during the optimizations. Inclusion of solvent effects (water) during the geometry optimizations has a minor impact in the calculated bond distances of the metal coordination environments (Tables S2−S4, Supporting Information), and therefore the data reported in this work were obtained using the geometries optimized in the gas phase. The stationary points found on the potential energy surfaces as a result of geometry optimizations were tested to represent energy minima rather than saddle points via frequency analysis. Gibbs free energies were obtained at T = 298.15 K within the harmonic approximation. The ΔG_g values reported in this work include basis-set superposition errors, which were estimated using the Counterpoise method of Boys and Bernardi (Table S5, Supporting Information).[62] The default values for the integration grid (75 radial shells and 302 angular points) and the SCF energy convergence criteria (10^{-8}) were used in all calculations.

Throughout this work solvent effects were included by using the polarizable continuum model (PCM), in which the solute cavity is built as an envelope of spheres centered on atoms or atomic groups with appropriate radii. In particular, the integral equation formalism (IEFPCM) variant as implemented in Gaussian 09 was used.[63] Hydration free energies were obtained using the radii and non-electrostatic terms obtained by Truhlar et al. (SMD solvation model).[64] The radii used for the Ln^{3+} ions were parametrized in a previous paper.[43] For Eu^{2+} we used a PCM radius of 1.876 Å, which provides a hydration free energy of −351.12 kcal mol^{-1}. This value compares well with the experimental one of −354.2 kcal mol^{-1} obtained assuming an absolute hydration free energy of the H^+ ion of −264.0 kcal mol^{-1}.[47,48]

■ ASSOCIATED CONTENT

Supporting Information

X-ray crystallographic data in CIF format, ^1H and ^{13}C NMR spectra, ESI^+ HR-MS, relative free energies of the $\Delta(\delta\lambda\delta)(\delta\lambda\delta)$ and $\Delta(\lambda\delta\lambda)(\lambda\delta\lambda)$ isomers, potentiometric curves, calculated bond distances of the metal coordination environments, cyclic voltammetry experiments, hydrogen-bonding data for bpa18c6·6H_2O, and optimized Cartesian coordinates obtained with DFT calculations. The Supporting Information is available free of charge on the ACS Publications website at DOI: 10.1021/acs.inorgchem.5b00548.

■ AUTHOR INFORMATION

Corresponding Author

*E-mail: carlos.platas.iglesias@udc.es.

Notes

The authors declare no competing financial interest.

■ ACKNOWLEDGMENTS

M. R.-F., D. E.-G., A.d.B., T. R.-B., and C. P.-I. thank Xunta de Galicia (CN 2012/011) and Universidade da Coruña for generous financial support and Centro de Supercomputación de Galicia (CESGA) for providing the computer facilities. E.T. acknowledges support of the Ligue National Contre le Cancer.

■ REFERENCES

(1) Seitz, M.; Oliver, A. G.; Raymond, K. N. *J. Am. Chem. Soc.* **2007**, *46*, 351−353.

(2) *Lanthanide Probes in Life, Chemical and Earth Sciences, Theory and Practice*; Bünzli, J.-C. G., Choppin, G. R., Eds.; Elsevier: Amsterdam, 1989.

(3) Garcia, J.; Allen, M. J. *Eur. J. Inorg. Chem.* **2012**, 4550−4563.

(4) (a) Gansow, O. A.; Kausar, A. R.; Triplett, K. M.; Weaver, M. J.; Yee, E. L. *J. Am. Chem. Soc.* **1977**, *99*, 7087−7089. (b) Yee, E. L.; Gansow, O. A.; Weaver, M. J. *J. Am. Chem. Soc.* **1980**, *102*, 2278−2285.

(5) Lehn, J. M. *Acc. Chem. Res.* **1978**, *11*, 49−57.

(6) (a) Sabbatini, N.; Ciano, M.; Dellonte, S.; Bonazzi, A.; Bolleta, F.; Balzani, V. *J. Phys. Chem.* **1984**, *88*, 1534−1537. (b) Sabbatini, N.; Ciano, M.; Dellonte, S.; Bonazzi, A.; Balzani, V. *Chem. Phys. Lett.* **1982**, *90*, 265−268.

(7) Burai, L.; Scopelliti, R.; Tóth, É. *Chem. Commun.* **2002**, 2366−2367.

(8) *The Chemistry of Contrast Agents in Medical Magnetic Resonance Imaging*, 2nd ed.; Merbach, A. E., Helm, L., Tóth, É., Eds.; Wiley: New York, 2013.

DOI: 10.1021/acs.inorgchem.5b00548
Inorg. Chem. 2015, 54, 4940−4952

(9) Burai, L.; Tóth, É.; Moreau, G.; Sour, A.; Scopelliti, R.; Merbach, A. E. *Chem.—Eur. J.* **2003**, *9*, 1394−1404.
(10) Seibig, S.; Tóth, É.; Merbach, A. E. *J. Am. Chem. Soc.* **2000**, *122*, 5822−5830.
(11) Burai, L.; Tóth, É.; Seibig, S.; Scopelliti, R.; Merbach, A. E. *Chem.—Eur. J.* **2000**, *6*, 3761−3770.
(12) Gamage, N.-D. H.; Mei, Y.; Garcia, J.; Allen, M. J. *Angew. Chem., Int. Ed.* **2010**, *49*, 8923.
(13) Garcia, J.; Kuda-Wedagedara, A. N. W.; Allen, M. J. *Eur. J. Inorg. Chem.* **2012**, 2135−2140.
(14) Ekanger, L. A.; Ali, M. M.; Allen, M. J. *Chem. Commun.* **2014**, *50*, 14835−14838.
(15) Garcia, J.; Allen, M. J. *Inorg. Chim. Acta* **2012**, *393*, 324−327.
(16) Roca-Sabio, A.; Mato-Iglesias, M.; Esteban-Gómez, D.; Tóth, É.; de Blas, A.; Platas-Iglesias, C.; Rodríguez-Blas, T. *J. Am. Chem. Soc.* **2009**, *131*, 3331−3341.
(17) Jensen, M. P.; Chiarizia, R.; Shkrob, I. A.; Ulicki, J. S.; Spindler, B. D.; Murphy, D. J.; Hossain, M.; Roca-Sabio, A.; Platas-Iglesias, C.; de Blas, A.; Rodríguez-Blas, T. *Inorg. Chem.* **2014**, *53*, 6003−6012.
(18) Shannon, R. D. *Acta Crystallogr.* **1976**, *A32*, 751−767.
(19) Ferreirós-Martínez, R.; Esteban-Gómez, D.; Tóth, É.; de Blas, A.; Platas-Iglesias, C.; Rodríguez-Blas, T. *Inorg. Chem.* **2011**, *50*, 3772−3784.
(20) Pearson, R. G. *J. Am. Chem. Soc.* **1963**, *85*, 3533−3539.
(21) (a) Wang, J.; Xiang, J.; Wu, A.; Meng, X. *CrystEngComm* **2013**, *15*, 10079−10085. (b) Etter, M. C. *J. Phys. Chem.* **1991**, *95*, 4601−4610.
(22) Shestakova, A. K.; Chertkov, V. A.; Schneider, H.-J.; Lysenko, K. A. *Org. Lett.* **2001**, *3*, 325−327.
(23) Platas, C.; Avecilla, F.; de Blas, A.; Rodríguez-Blas, T.; Bastida, R.; Macías, A.; Rodríguez, A.; Adams, H. *J. Chem. Soc., Dalton Trans.* **2001**, 1699−1705.
(24) Saleh, M. I.; Salhin, A.; Saad, B.; Zain, S. M.; Arifin, Z. *J. Mol. Struct.* **1997**, *415*, 71−79.
(25) Bombieri, G.; Marchini, N.; Ciattini, S.; Mortillaro, A.; Aime, S. *Inorg. Chim. Acta* **2006**, *359*, 3405−3411.
(26) Esteban-Gomez, D.; de Blas, A.; Rodríguez-Blas, T.; Helm, L.; Platas-Iglesias, C. *ChemPhysChem* **2012**, *13*, 3640−3650.
(27) (a) Corey, E. J.; Bailar, J. C., Jr. *J. Am. Chem. Soc.* **1959**, *81*, 2620−2629. (b) Beattie, J. K. *Acc. Chem. Res.* **1971**, *4*, 253−259.
(28) Aime, S.; Botta, M.; Fasano, M.; Marques, M. P. M.; Geraldes, C. F. G. C.; Pubanz, D.; Merbach, A. E. *Inorg. Chem.* **1997**, *36*, 2059−2068.
(29) De Sousa, A. S.; Hancock, R. D.; Reibenspies, J. H. *J. Chem. Soc., Dalton Trans.* **1997**, 939−944.
(30) Carreira-Barral, I.; Rodríguez-Rodríguez, A.; Regueiro-Figueroa, M.; Esteban-Gómez, D.; Platas-Iglesias, C.; de Blas, A.; Rodríguez-Blas, T. *Inorg. Chim. Acta* **2011**, *370*, 270−278.
(31) Bühl, M.; Sieffert, N.; Chaumont, A.; Wipff, G. *Inorg. Chem.* **2011**, *50*, 299−308.
(32) Rodríguez-Rodríguez, A.; Esteban-Gómez, D.; de Blas, A.; Rodríguez-Blas, T.; Fekete, M.; Botta, M.; Tripier, R.; Platas-Iglesias, C. *Inorg. Chem.* **2012**, *51*, 2509−2521.
(33) Doffek, C.; Alzakhem, N.; Bischof, C.; Wahsner, J.; Güden-Silber, T.; Lügger, J.; Platas-Iglesias, C.; Seitz, M. *J. Am. Chem. Soc.* **2012**, *134*, 16413−16423.
(34) Peters, J. A.; Huskens, J.; Raber, D. J. *Prog. Nucl. Magn. Reson. Spectrosc.* **1996**, *28*, 283−350.
(35) Forsberg, J. H.; Delaney, R. M.; Zhao, Q.; Harakas, G.; Chandran, R. *Inorg. Chem.* **1995**, *34*, 3705−3715.
(36) (a) Liu, T.; Nonat, A.; Beyler, M.; Regueiro-Figueroa, M.; Nono, K. N.; Jeannin, O.; Camerel, F.; Debaene, F.; Cianférani-Sanglier, S.; Tripier, R.; Platas-Iglesias, C.; Charbonnière, L. J. *Angew. Chem., Int. Ed.* **2014**, *53*, 7259−7263. (b) Rodríguez-Rodríguez, A.; Esteban-Gómez, D.; Tripier, R.; Tircsó, G.; Garda, Z.; Tóth, I.; de Blas, A.; Rodríguez-Blas, T.; Platas-Iglesias, C. *J. Am. Chem. Soc.* **2014**, *136*, 17954−17957.
(37) $AF_j = [\sum_i(\delta_i^{exp} - \delta_i^{cal})^2/\sum_i(\delta_i^{exp})^2]^{1/2}$, where δ_i^{exp} and δ_i^{cal} represent the experimental and calculated values of a nucleus *i*, respectively. (a) Willcott, M. R.; Lenkinski, R. E.; Davis, R. E. *J. Am. Chem. Soc.* **1972**, *94*, 1742−1744. (b) Davis, R. E.; Willcott, M. R. *J. Am. Chem. Soc.* **1972**, *94*, 1744−1745.
(38) Brücher, E.; Györi, B.; Emri, J.; Solymosi, P.; Sztanyik, L. B.; Varga, L. *J. Chem. Soc., Chem. Commun.* **1993**, 574−575.
(39) Chang, C. A.; Rowland, M. E. *Inorg. Chem.* **1983**, *22*, 3866−3869.
(40) Palinkas, Z.; Roca-Sabio, A.; Mato-Iglesias, M.; Esteban-Gomez, D.; Platas-Iglesias, C.; de Blas, A.; Rodriguez-Blas, T.; Toth, E. *Inorg. Chem.* **2009**, *48*, 8878−8889.
(41) (a) Chatterton, N.; Gateau, C.; Mazzanti, M.; Pecaut, J.; Borel, A.; Helm, L.; Merbach, A. E. *Dalton Trans.* **2005**, 1129−1135. (b) Ferreirós-Martínez, R.; Esteban-Gómez, D.; Platas-Iglesias, C.; de Blas, A.; Rodríguez-Blas, T. *Dalton Trans.* **2008**, 5754−5765.
(42) Kálmán, F. K.; Végh, A.; Regueiro-Figueroa, M.; Tóth, E.; Platas-Iglesias, C.; Tircsó, G. *Inorg. Chem.* **2015**, *54*, 2345−2356.
(43) Regueiro-Figueroa, M.; Esteban-Gómez, D.; de Blas, A.; Rodríguez-Blas, T.; Platas-Iglesias, C. *Chem.—Eur. J.* **2014**, *20*, 3974−3981.
(44) Mato-Iglesias, M.; Roca-Sabio, A.; Pálinkás, Z.; Esteban-Gómez, D.; Platas-Iglesias, C.; Tóth, É.; de Blas, A.; Rodríguez-Blas, T. *Inorg. Chem.* **2008**, *47*, 7840−7851.
(45) (a) Botta, M.; Ravera, M.; Barge, A.; Bottaro, M.; Osella, D. *Dalton. Trans.* **2003**, 1628−1633. (b) Gal, M.; Kielar, F.; Sokolova, R.; Ramesova, S.; Kolivoska, V. *Eur. J. Inorg. Chem.* **2013**, 3217−3223.
(46) Cosentino, U.; Villa, A.; Pitea, D.; Moro, G.; Barone, V. *J. Phys. Chem. B* **2000**, *104*, 8001−8007.
(47) Marcus, Y. *J. Chem. Soc., Faraday Trans.* **1991**, *87*, 2995−2999.
(48) Tissandier, M. D.; Cowen, K. A.; Feng, W. Y.; Gundlach, E.; Cohen, M. H.; Earhart, A. D.; Coe, J. V. *J. Phys. Chem. A* **1998**, *102*, 7787−7794.
(49) Halliwell, B.; Gutteridge, J. M. C. *Free Radicals in Biology and Medicine*, 4th ed.; Oxford University Press: Oxford, U.K., 2007.
(50) Friis, E. P.; Andersen, J. E. T.; Madsen, L. L.; Bonander, N.; Moller, P.; Ulstrup, J. *Electrochim. Acta* **1998**, *43*, 1114−1122.
(51) Martell, A. E.; Motekaitis, R. J. *Determination and Use of Stability Constants*; VCH: New York, 1992.
(52) Gans, P.; Sabatini, A.; Vacca, A. *Talanta* **1996**, *43*, 1739−1753.
(53) Smith, R. M.; Motekaitis, R. J.; Martell, A. E. *NIST Standard Reference Database*; National Institute of Standards and Technology: Gaithersburg, MD, 1997.
(54) Sheldrick, G. M. *SADABS Version 2.10*; University of Göttingen: Göttingen, Germany, 2004.
(55) Sheldrick, G. M. *Acta Crystallogr., Sect. A* **2008**, *64*, 112−122.
(56) Farrugia, L. J. *J. Appl. Crystallogr.* **1999**, *32*, 837−838.
(57) Burla, M. C.; Caliandro, R.; Camalli, M.; Carrozzini, B.; Cascarano, G. L.; Giacovazzo, C.; Mallamo, M.; Mazzone, A.; Polidori, G.; Spagna, R. *J. Appl. Crystallogr.* **2012**, *45*, 357−361.
(58) Beurskens, P. T.; Beurskens, G.; de Gelder, R.; Smits, J. M. M.; Garcia-Granda, S.; Gould, R. O. *DIRDIF2008*; Crystallography Laboratory, Radboud University Nijmegen: Nijmegen, The Netherlands, 2008.
(59) Frisch, M. J.; Trucks, G. W.; Schlegel, H. B.; Scuseria, G. E.; Robb, M. A.; Cheeseman, J. R.; Scalmani, G.; Barone, V.; Mennucci, B.; Petersson, G. A.; Nakatsuji, H.; Caricato, M.; Li, X.; Hratchian, H. P.; Izmaylov, A. F.; Bloino, J.; Zheng, G.; Sonnenberg, J. L.; Hada, M.; Ehara, M.; Toyota, K.; Fukuda, R.; Hasegawa, J.; Ishida, M.; Nakajima, T.; Honda, Y.; Kitao, O.; Nakai, H.; Vreven, T.; Montgomery, J. A., Jr.; Peralta, J. E.; Ogliaro, F.; Bearpark, M.; Heyd, J. J.; Brothers, E.; Kudin, K. N.; Staroverov, V. N.; Kobayashi, R.; Normand, J.; Raghavachari, K.; Rendell, A.; Burant, J. C.; Iyengar, S. S.; Tomasi, J.; Cossi, M.; Rega, N.; Millam, N. J.; Klene, M.; Knox, J. E.; Cross, J. B.; Bakken, V.; Adamo, C.; Jaramillo, J.; Gomperts, R.; Stratmann, R. E.; Yazyev, O.; Austin, A. J.; Cammi, R.; Pomelli, C.; Ochterski, J. W.; Martin, R. L.; Morokuma, K.; Zakrzewski, V. G.; Voth, G. A.; Salvador, P.; Dannenberg, J. J.; Dapprich, S.; Daniels, A. D.; Farkas, Ö.; Foresman, J. B.; Ortiz, J. V.; Cioslowski, J.; Fox, D. J. *Gaussian 09, Revision D.01*; Gaussian, Inc.: Wallingford, CT, 2009.

DOI: 10.1021/acs.inorgchem.5b00548
Inorg. Chem. 2015, 54, 4940−4952

(60) Tao, J. M.; Perdew, J. P.; Staroverov, V. N.; Scuseria, G. E. *Phys. Rev. Lett.* **2003**, *91*, 146401.
(61) Dolg, M.; Stoll, H.; Savin, A.; Preuss, H. *Theor. Chim. Acta* **1989**, *75*, 173−194.
(62) Bernardi, F.; Boys, S. F. *Mol. Phys.* **1970**, *19*, 553−566.
(63) Tomasi, J.; Mennucci, B.; Cammi, R. *Chem. Rev.* **2005**, *105*, 2999−3093.
(64) Marenich, A. V.; Cramer, C. J.; Truhlar, D. G. *J. Phys. Chem. B* **2009**, *113*, 6378−6396.

DOI: 10.1021/acs.inorgchem.5b00548
Inorg. Chem. 2015, 54, 4940−4952